Forced obliquity variations of Mercury

Bruce G. Bills

NASA Goddard Space Flight Center, Greenbelt, Maryland, USA

Scripps Institution of Oceanography, La Jolla, California, USA

Robert L. Comstock

Scripps Institution of Oceanography, La Jolla, California, USA

[1] The spin pole of Mercury is very nearly, but not quite, aligned with its orbit pole. Tidal dissipation has driven the free obliquity to very small values, and the high rate of spin pole precession allows the forced obliquity variations to remain small despite significant variations in orbital inclination and eccentricity. We present calculations of the obliquity for a 10 million year time span, centered on the present. The obliquity remains small, with typical values of 2–4 minutes of arc. The dominant period of obliquity oscillations is 895 kyr, which is also the main period at which the orbital inclination varies. If the orbit pole precession rate were uniform, dissipation would have driven Mercury into a Cassini state, in which the spin pole and orbit pole remain coplanar with the invariable pole, as the spin pole precesses about the moving orbit pole. However, due to the nonuniform orbit precession rate, this simple coplanar configuration is not maintained, except on a mode-by-mode basis. That is, when the orbit pole motion is represented as a sum of normal modes of the coupled oscillations of the planetary system, the spin pole coprecesses with the orbit pole at each modal frequency. This is a generalization of Cassini's second and third laws of lunar rotation to the case of nonuniform orbit precession. We compare results of a linearized obliquity model with a numerical integration of the equations of motion. The two solutions agree at the level of a few seconds of arc.

1. Introduction

[2] Tidal dissipation within Mercury has quite dramatically influenced that planet's rotation. In addition to occupying the only known case of a nonsynchronous spin-orbit resonance [*Pettengill and Dyce*, 1965], Mercury also has the distinction of the smallest known value of planetary obliquity [*Klaasen*, 1976; *Harmon et al.*, 2001], or angular separation between the spin pole and the instantaneous orbit pole. Tidal dissipation has driven the spin pole to a state in which it is very nearly parallel to the orbit normal. Considerable effort has been devoted to understanding the origin of the spin-orbit resonance [*Colombo and Shapiro*, 1966; *Goldreich and Peale*, 1966, 1968] and the unusual obliquity state [*Colombo*, 1966; *Peale*, 1969, 1974, 1976; *Peale and Boss*, 1977a, 1977b; *Ward*, 1975; *Henrard and Murigande*, 1987]. After several decades of relative neglect, two spacecraft missions to Mercury are being planned [*Solomon et al.*, 2001; *Peale et al.*, 2002; *Balogh and Giampieri*, 2002; *Anselmi and Scoon*, 2001; *Milani et al.*, 2001], and innovative radar investiga-

tions are providing improved constraints on the current rotation state [*Holin*, 2002].

[3] In anticipation of a wealth of dynamically relevant information in the near future, our objective is to examine a simple model of the orbital and rotational variations of Mercury over a relatively short period of time near the present, and attempt to understand how the obliquity is currently varying. For a perfectly spherical body, there would be no gravitational torque and the spin pole would remain fixed in inertial space. In that case, any variation in the orientation of the orbit plane would be directly manifest as obliquity variations. For an oblate planet, gravitational torques cause the spin pole to precess about the instantaneous orbit pole, and obliquity variations reflect changes in either the orbit pole, the spin pole, or both. The spin pole precession rate can be estimated by equating the change in angular momentum to the applied torque. For a rapidly rotating body, this torque balance can be written as [*Ward*, 1973, 1992; *Kinoshita*, 1977; *Bills*, 1990]

$$\frac{d\hat{s}}{dt} = \frac{\alpha}{(1-e^2)^{3/2}} \, (\hat{n} \cdot \hat{s}) \, (\hat{s} \times \hat{n}), \tag{1}$$

where $\hat{s}$ and $\hat{n}$ are unit vectors along the spin pole and orbit normal respectively, e is the orbital eccentricity, and α is a scalar rate parameter which depends on the principal moments of inertia $A < B < C$, the spin rate σ, and the orbital mean motion n, via

$$\alpha = \frac{3}{2}\left(\frac{C-(A+B)/2}{C}\right)\frac{n^2}{\sigma}. \qquad (2)$$

To model the spin precession of a resonant rotator, like Mercury, we will need to make some modifications to this formula. However, as we will see in the next section, the basic form will remain quite similar.

[4] In order to explore the dynamics of spin pole variations we obviously need a representation of the variations in orbital inclination and eccentricity, and an estimate of the parameter α. The net effect of the spin pole motion, as given in equation (1), is that the spin pole $\hat{s}$ precesses about the instantaneous orbit pole $\hat{n}$. If the orbit pole and eccentricity were both fixed, then the spin pole would trace out a circular trajectory centered on the orbit pole, and the obliquity would remain constant.

[5] If the orbit pole of Mercury were precessing at a steady rate, and at fixed inclination to the solar system invariable plane, the effect of tidal dissipation would be to drive the spin pole to a configuration in which the spin pole and orbit pole would remain coplanar with the solar system invariable pole [Colombo, 1966; Peale, 1969; Ward, 1975; Henrard and Murigande, 1987]. That configuration represents a generalization of Giovanni Cassini's second and third laws governing the rotational motion of the Moon [Cassini, 1693]. In that case the obliquity would also remain constant.

[6] However, Mercury's orbit pole precession rate is quite irregular, and the spin pole cannot remain coplanar with the orbit pole and the invariable pole. Instead, the effect of tidal dissipation is to drive the system toward a state in which the obliquity varies, but in a particularly simple way. A linearized analysis of the equations of precessional motion indicates that for each mode of oscillation in the orbit pole, there is a corresponding mode of spin pole oscillation. The orbit and spin modes have identical frequencies and phases, and the amplitudes are related via a simple linear filter. The coplanar configuration of spin pole, orbit pole and invariable pole is maintained on a mode-by-mode basis.

[7] It is informative, in this context, to compare the obliquity variations of Mercury with those of Earth and Mars. Both Earth and Mars have reasonably large mean obliquity values, but Earth's obliquity has only quite small amplitude variations about the mean whereas Mars exhibits much larger amplitude variations in its obliquity [Ward and Rudy, 1991; Touma and Wisdom, 1993; Laskar and Robutel, 1993]. This difference has a simple explanation. The orbital inclination variations of Mars and Earth are quite similar in amplitude, and have identical frequencies of oscillation. The difference in obliquity variations is due to the fact that the spin pole precession rate parameter of Mars ($\alpha = 7.6$ arcsec/year) [Folkner et al., 1997; Yoder et al., 2003] is comparable to some of the rates at which the orbit pole precesses, and there is a resonant amplification of the spin precession. For Earth, the spin pole precession rate parameter is much higher ($\alpha = 50.29$ arcsec/year) [Williams, 1994; McCarthy

and Luzum, 2003] and there are no significant orbital motions in that frequency range. The mean obliquity of Mercury is small, as a result of tidal dissipation, and the variations about the mean are also small because the spin pole precesses much more rapidly than the orbit pole. Mercury, in that regard, is more similar to Earth than to Mars.

[8] A potentially important way in which Mercury differs from either Earth or Mars is that the orbital inclination and eccentricity variations are quite large. Linear models of the spin pole's response to orbital variations provide a good description of the actual behavior for Earth, and somewhat less so for Mars. Though the variations in obliquity for Mercury are expected to remain small, it is not obvious a priori how well the linear model will perform. We thus compare estimates of the spin pole behavior in linear and nonlinear models.

[9] Another way in which Mercury differs from Earth and Mars is that the present orientation of the spin pole is still only rather poorly known. Until very recently, the best estimates of the spin pole orientation of Mercury were obtained from Mariner 10 observations [Klaasen, 1976] and Earth-based radar range measurements [Anderson et al., 1996]. Recent work [Holin, 2002], using radar speckle interferometry is dramatically improving the situation, and the current spin pole orientation should be known to an accuracy of a few arcseconds within a few years. In modeling spin pole dynamics of bodies like Earth and Mars, the present orientation of the spin pole is imposed as an initial condition. For Mercury, the expected departure of the spin pole from the orbit normal is smaller than the current uncertainty. However, the fact that tidal dissipation has driven the spin pole close to the orbit normal can be exploited to yield a dynamically consistent solution without any dependence on initial conditions. In effect, we assume that the free obliquity of Mercury is zero, and the only deviations between the orbit normal and spin pole are forced by the orbital motion.

[10] The remainder of this paper is divided into 6 sections. In section 2 we develop a simple model for spin pole precession, after averaging the gravitational solar torque over the orbital and rotational periods. In section 3 we estimate the spin pole precession rate parameters. In section 4 we discuss the secular orbital model. In section 5 we develop a linear model of spin pole variations, in response to solar torques and variations in orbit pole orientation. In section 6 we present results of numerical integration of the equations of motion. In section 7 we summarize and discuss the results.

2. Spin Precession Model

[11] In this section we develop a simple representation of the precession of the spin pole of Mercury, under the influence of solar torques. Equation (1), given in section 1, is strictly correct only for rapidly rotating bodies, in which departures from symmetry about the rotation axis play no role. For synchronous rotators, like the Moon, or for resonant rotators like Mercury, the departure from axial symmetry modifies the torque balance, and must be properly accounted for. We will see, however, that the

proper torque balance equation for Mercury can be written in a form rather similar to that for a rapid rotator.

[12] The precession of the spin pole of a planet or satellite can be modeled quite simply by equating the change in spin angular momentum to the applied gravitational torque. The instantaneous gravitational torque acting on a triaxial body due to a distant point mass can be written in the form

$$T = \frac{3\mu}{r^3} \ (\widehat{u} \times I \cdot \widehat{u}), \tag{3}$$

in which the gravitational monopole moment of the source is

$$\mu = G \ m_s, \tag{4}$$

where G is the gravitational constant and m_s is the source mass, r is the distance from the rotator to the source, I is the inertia tensor of the triaxial body, and $\widehat{u}$ is a unit vector oriented toward the source, as seen from the center of the rotator. This formulation yields both short period torques, which give rise to nutations and librations, and long period torques which cause the precession we are mainly interested in. For recent accounts of the short period effects, see *Rambaux and Bois* [2004] and *Carpentier and Roosbeek* [2003].

[13] If the triaxial body and point source are in a binary orbit, and the torques are averaged over the rotation period and orbital period of the body, we can write the precession equation in the form

$$\frac{d \widehat{s}}{d t} = \frac{3}{2} \left(\frac{n^2}{\sigma} \right) (\alpha^* \ (\widehat{n} \cdot \widehat{s}) + \beta^*)(\widehat{s} \times \widehat{n}), \tag{5}$$

where $\widehat{n}$ and $\widehat{s}$ are unit vectors along the orbit pole and spin pole, respectively, n and σ are the rates of mean orbital motion and rotation of the triaxial body, and α^* and β^* are functions of the orbital eccentricity e and the principal moments of inertia ($A < B < C$). The particular forms taken by the dimensionless parameters α^* and β^* depend on the relative rates of rotational and orbital motion, a point to which we will return momentarily.

[14] Several features of this formulation deserve comment. All but the terms within the first set of parentheses are dimensionless. The direction of the precessional motion is dependent only on the two unit vectors $\widehat{n}$ and $\widehat{s}$, and is perpendicular to both of them, due to the $\widehat{s} \times \widehat{n}$ term. The orbital mean motion n is related to source strength μ and orbital semimajor axis a via Kepler's third law:

$$a^3 n^2 = \mu(1 + \nu), \tag{6}$$

where the mass ratio is

$$\nu = \frac{m}{m_s} \tag{7}$$

and m is the mass of the rotator. For small mass ratios ($\nu \ll 1$) we can make the approximation

$$\frac{\mu}{a^3} = n^2, \tag{8}$$

which was employed in writing equation (5).

[15] In averaging the torques, we need to write functions of orbital radius r and orbital true anomaly f in terms of orbital mean anomaly M, which varies linearly with time. A convenient format for such expansions was introduced by *Cayley* [1861]. He tabulated expansion coefficients for functions of the form

$$\left(\frac{r}{a} \right)^p \cos(qf) = \sum_{j=0}^{\infty} \mathcal{C}_j^{p,q}[e] \cos(jM), \tag{9}$$

$$\left(\frac{r}{a} \right)^p \sin(qf) = \sum_{j=0}^{\infty} \mathcal{S}_j^{p,q}[e] \sin(jM), \tag{10}$$

where p and q are integers and the coefficients $\mathcal{C}_j^{p,q}$ and $\mathcal{S}_j^{p,q}$ are functions of orbital eccentricity e. Explicitly, those coefficients are given by the integrals

$$\mathcal{C}_j^{p,q}[e] = \frac{1}{2\pi} \int_0^{2\pi} \left(\frac{r}{a} \right)^p \cos(qf) \cos(jM) \ dM, \tag{11}$$

$$\mathcal{S}_j^{p,q}[e] = \frac{1}{2\pi} \int_0^{2\pi} \left(\frac{r}{a} \right)^p \sin(qf) \sin(jM) \ dM. \tag{12}$$

The evaluation of these integrals, though rather tedious for Cayley, is now readily implemented via recurrence relations [*Hughes*, 1981; *Vakhidov*, 2001].

[16] If the rotation angle of the axis of least inertia of the triaxial body is

$$s = \tau + b \ M, \tag{13}$$

where τ is the angle, measured from the ascending node of the orbit on the equator plane at periapse, and b is a half integer, then we will need three coefficients: $\mathcal{C}_0^{-3,0}[e]$, $\mathcal{C}_{2b}^{-3,2b}[e]$, and $\mathcal{S}_{2b}^{-3,2b}[e]$. The first of these has a simple closed-form expression:

$$\mathcal{C}_0^{-3,0}[e] = \left(1 - e^2 \right)^{-3/2}. \tag{14}$$

The others are given in terms of Taylor series expansions, with different forms for each value of the spin-orbit rate ratio b.

[17] The most familiar form of the precessional equation is that which is applicable to rapid rotators, such as Earth or Mars. In that case, the torques can be averaged over the spin period, holding the orbital position fixed, and then separately averaged over the orbital position angle. In that case the dimensionless parameters α^* and β^* are given by

$$\alpha^* c = J_2 \ \mathcal{C}_0^{-3,0}[e]$$
$$= J_2 \left(1 + \frac{3}{2} e^2 + \cdots \right), \tag{15}$$

$$\beta^* = 0, \tag{16}$$

where J_2 is the degree two zonal harmonic coefficient of the gravitational potential of the rotator, which is related to the

principal moments (A, B, C), mass m and mean radius R of the body via

$$J_2 \, m \, R^2 = C - \left(\frac{A+B}{2}\right), \tag{17}$$

and c is the dimensionless polar moment of inertia:

$$c = \frac{C}{m \, R^2}. \tag{18}$$

[18] For a synchronous rotator, in which $b = 1$, the torque averaging is still a simple calculation, but is somewhat more tedious. After adjusting the phase angle τ so that the mean torque about the spin axis vanishes (in order to maintain synchronous rotation), the result can be written as

$$\alpha^* c = J_2 \, C_0^{-3,0}[e] + C_{2,2} \, C_2^{-3,2}[e], \tag{19}$$

$$\beta^* c = -C_{2,2} \, C_2^{-3,2}[e], \tag{20}$$

where $C_{2,2}$ is a harmonic coefficient of degree two and order two in the potential of the rotator, and is given by

$$C_{2,2} \, m \, R^2 = \left(\frac{B-A}{4}\right). \tag{21}$$

Note that the rapid rotator has no term proportional to the difference in equatorial moments, as the spin averaging is equivalent to setting $A = B$. If we truncate the Cayley coefficient expansions at second degree in eccentricity, we have for the synchronous case

$$\alpha^* c = J_2 \left(1 + \frac{3}{2} e^2\right) + C_{2,2} \left(1 - \frac{5}{2} e^2\right), \tag{22}$$

$$\beta^* c = -C_{2,2} \left(1 - \frac{5}{2} e^2\right). \tag{23}$$

[19] The result for a 3:2 spin-orbit resonance is quite similar to the synchronous case:

$$\alpha^* c = J_2 \, C_0^{-3,0}[e] + C_{2,2} \, C_3^{-3,3}[e], \tag{24}$$

$$\beta^* c = -C_{2,2} \, C_3^{-3,3}[e]. \tag{25}$$

The only difference is that the gravitation potential coefficient $C_{2,2}$ is multiplied by a different Cayley coefficient. Again truncating the Cayley coefficients at second degree in eccentricity, we obtain

$$\alpha^* c = J_2 \left(1 + \frac{3}{2} e^2\right) + C_{2,2} \left(1 - 5 e^2\right), \tag{26}$$

$$\beta^* c = -C_{2,2} \left(1 - 5 e^2\right). \tag{27}$$

[20] If the obliquity is small enough that

$$\widehat{n} \cdot \widehat{s} \simeq 1, \tag{28}$$

then the precession formula can be written as

$$\frac{d\widehat{s}}{dt} = \frac{3}{2} \left(\frac{n^2}{\sigma}\right) Q[e] \, (\widehat{s} \times \widehat{n}), \tag{29}$$

with

$$Q[e] = (\alpha^* + \beta^*). \tag{30}$$

We will see below that this small angle approximation is very well justified for Mercury.

[21] If the Taylor series expansion in orbital eccentricity e is truncated at degree two, we can write

$$\frac{d\widehat{s}}{dt} = \left(\alpha_0 + \alpha_2 \, e^2\right)(\widehat{s} \times \widehat{n}). \tag{31}$$

The rapid rotator version of this formula can be written with

$$\alpha_0 = \frac{3}{2} \left(\frac{J_2}{c}\right) \left(\frac{n}{\sigma}\right) n, \tag{32}$$

$$\alpha_2 = \frac{9}{4} \left(\frac{J_2}{c}\right) \left(\frac{n}{\sigma}\right) n = \frac{3}{2} \alpha_0. \tag{33}$$

The corresponding form for Mercury, with $2\sigma = 3n$ is

$$\alpha_0 = \left(\frac{J_2}{c}\right) n, \tag{34}$$

$$\alpha_2 = \frac{3}{2} \left(\frac{J_2}{c}\right) n. \tag{35}$$

[22] We thus see that, if we only retain terms of first order in obliquity and second order in eccentricity, the resonant rotator and rapid rotator versions of the precession equation are almost identical in form. Analyses of the dynamical evolution of Mercury into its present low-obliquity configuration [Peale, 1974; Peale and Boss, 1977a, 1977b] are obliqated to consider the higher order terms, but for treatment of the present situation, this simpler form is quite adequate.

3. Spin Pole Precession Rate

[23] In this section we estimate the numerical values of the spin pole precession rate parameters of Mercury. These parameters play an important role in the obliquity calculation since they determine how well the spin pole can track changes in the orientation of the orbit pole. Examination of the formulas for these parameters, given just above, reveals that they are each a combination of spin and orbit rate parameters, which are very well known, and a moment difference ratio which is not yet well determined. The best

known of the input parameters is the orbital mean motion [*Standish et al.*, 1992]:

$$n = 5,381,016.2829 \text{ arcsec/year.} \tag{36}$$

The spin rate is observed to be very close to 1.5 times the orbital mean motion [*Pettengill and Dyce*, 1965] and is presumed to be exactly in that resonance [*Goldreich and Peale*, 1966; *Colombo and Shapiro*, 1966; *Counselman*, 1969]:

$$\sigma = \frac{3}{2} n. \tag{37}$$

From perturbations in the trajectory of the Mariner 10 spacecraft, as it flew past Mercury in March and September of 1974 and again in March of 1975, it has been possible to estimate the required degree two harmonic coefficients of the gravitational potential [*Anderson et al.*, 1987]:

$$J_2 = (60 \pm 20) \times 10^{-6}, \tag{38}$$

$$C_{22} = (10 \pm 5) \times 10^{-6}, \tag{39}$$

where M and R are the mass and mean radius of the planet. The remaining parameter for which we need a value is the normalized polar moment of inertia:

$$c = \frac{C}{M R^2}. \tag{40}$$

There are no direct observational constraints on this parameter, but arguments based on analogy with Earth suggest that [*Schubert et al.*, 1988; *Harder and Schubert*, 2001; *Spohn et al.*, 2001]

$$c = 0.35 \pm 0.02. \tag{41}$$

Combining these input values, we obtain estimates of

$$\alpha_0 = \left(\frac{J_2}{c}\right) n = (922 \pm 312) \text{ arcsec/year,} \tag{42}$$

$$\alpha_2 = \frac{3}{2}\left(\frac{J_2}{c}\right) n = (1384 \pm 468) \text{ arcsec/year.} \tag{43}$$

Though the uncertainty in these critical parameters is quite large, the probable range of values are all substantially larger than any of the secular orbital precession rates. As a result, the amplitude of the forced obliquity variations will be very nearly inversely proportional to the net precession rate parameter. By planetary standards, the eccentricity of Mercury's orbit is quite high. As will be seen in the next section, the long-term (10^7 year) average eccentricity is very nearly 0.2, though it can be as high as 0.3 or as low as 0.1.

The average value of the spin pole precession rate parameter will be

$$\langle\alpha\rangle = \alpha_0 + \alpha_2 \langle e\rangle^2 = (959 \pm 354) \text{ arcsec/year.} \tag{44}$$

4. Orbit Model

[24] In this section we describe the orbital model that will form the basis of our subsequent analyses. We employ a secular variation model [*Laskar*, 1988] which includes effects up to second order in masses and fifth order in inclination and eccentricity. For each body, the semimajor axis remains constant, and the shape and orientation of the orbit are described by parameter pairs eccentricity (e) and longitude of periapse (ϖ), and inclination (I) and longitude of the ascending node (Ω). The reference frame is the ecliptic and equinox of J2000. Any of a variety of other reference frames could be chosen, and for some analyses, it is even convenient to use a rotating or noninertial reference frame. However, for our analysis, it will greatly simplify matters to use an inertial frame.

[25] In a secular variation model, the interactions between the point-mass planets are averaged over their orbital periods, and the point masses are effectively replaced by gravitating hoops. In the lowest order models, the solutions for (e, ϖ) are decoupled from the solutions for (I, Ω), and there are as many modes of oscillation as there are interacting planets [*Brouwer and van Woerkom*, 1950; *Murray and Dermott*, 1999]. It will be convenient to use a new set of variables to describe the orbits. For each planet j, we define

$$h_j = e_j \sin \varpi_j, \tag{45}$$

$$k_j = e_j \cos \varpi_j, \tag{46}$$

and

$$p_j = \sin I_j \sin \Omega_j, \tag{47}$$

$$q_j = \sin I_j \cos \Omega_j. \tag{48}$$

Each of these parameters is represented by a Poisson series:

$$h_j(t) = \sum_{i=1}^{N} G_{ji} \sin(g_i t + \gamma_i), \tag{49}$$

$$k_j(t) = \sum_{i=1}^{N} G_{ji} \cos(g_i t + \gamma_i), \tag{50}$$

and

$$p_j(t) = \sum_{i=1}^{N} F_{ji} \sin(f_i t + \varphi_i), \tag{51}$$

$$q_j(t) = \sum_{i=1}^{N} F_{ji} \cos(f_i t + \varphi_i). \tag{52}$$

As written here, the index j identifies the planet and the index i corresponds to the mode of oscillation.

[26] Note that, despite their superficial resemblance to Fourier series, these are Poisson series. In either case, the series is a sum of sines and/or cosines of fixed frequencies and phases. However, in a Fourier series, all of the frequencies are integer multiples of a single base frequency. In the Poisson series, the frequencies have no simple relationship to each other. As a consequence, the orbital elements vary in a quasi-periodic fashion. For further discussion of Poisson series, see *Henrard* [1989], *Deprit and Deprit* [1990], *San Juan and Abad* [2001], and *Navarro and Ferrándiz* [2002].

[27] It is important to note that representing the slow temporal variations in orbital parameters via a Poisson series does not necessarily imply that the motion is actually quasiperiodic, rather than chaotic. The long term stability of orbital motion in the solar system has been a subject of intensive study for centuries, and is still not completely resolved [*Wisdom*, 1987; *Lissauer*, 1999; *Lecar et al.*, 2001; *Morbidelli*, 2002]. It is known that some of the orbital motions are chaotic, and all known cases of chaos in the solar system are due to overlapping resonances [*Chirikov*, 1979; *Wisdom*, 1980; *Winter and Murray*, 1997a, 1997b]. The inner solar system is particularly prone to chaotic motions [*Laskar*, 1990, 1994; *Sussman and Wisdom*, 1992; *Ito and Tanikawa*, 2002]. However, that does not preclude representing the motion over long periods of time via a quasiperiodic approximation. It is somewhat analogous to using the Keplerian orbital elements to describe the orbital trajectory, even though they are only fixed parameters for the isolated two-body problem.

[28] In the lowest order secular models, all of the frequencies g_j, which are associated with eccentricity and periapse, are positive, and the frequencies f_j, which are associated with inclination and node, are negative. As a result, the nodal lines regress and the apsidal lines advance. In a higher order secular model, there are more modes of oscillation. The current model includes 80 terms for each body. Figure 1 illustrates the amplitude spectra for the eccentricity and inclination series of Mercury. The largest inclination term has an angular rate of -5.60 arcsec/year, with a corresponding period of 231 kyr, and most of the other terms in the Poisson series have negative angular rates. The largest eccentricity term has a rate of 5.57 arcsec/year, with a corresponding period of 228 kyr, and most of the other terms are also positive. The eccentricity variations are more dominated by the largest single term than is the case for inclination.

[29] The scalar quantities eccentricity and inclination are obtained from the 2-vectors (h, k) and (p, q) via

$$e = \sqrt{h(t)^2 + k(t)^2}, \qquad (53)$$

$$\sin I = \sqrt{p(t)^2 + q(t)^2}. \qquad (54)$$

Similarly, the rates of change of the orbital elements are obtained via

$$\frac{d}{dt}\begin{bmatrix} e \\ \varpi \end{bmatrix} = \frac{1}{e^2}\begin{bmatrix} e\,h & e\,k \\ k & -h \end{bmatrix}\frac{d}{dt}\begin{bmatrix} h \\ k \end{bmatrix}, \qquad (55)$$

$$\frac{d}{dt}\begin{bmatrix} \sin I \\ \Omega \end{bmatrix} = \frac{1}{\sin^2 I}\begin{bmatrix} p\sin I & q\sin I \\ q & -p \end{bmatrix}\frac{d}{dt}\begin{bmatrix} p \\ q \end{bmatrix}. \qquad (56)$$

[30] Figure 2 illustrates the variations in inclination and eccentricity for Mercury for a 10 million year time span, centered on the present, as represented by the secular variation model. There are several features of note. The dominant period of oscillation in inclination is near 1 million years. This represents a beat between the two largest terms in the Poisson series. The rates of -5.604 and -7.053 arcsec/year yield a beat period of 895 kyr. The present inclination is near the long term average, but there is significant variability. The inclination history is very nearly symmetric about an epoch roughly 200 kyr ago. The cause and effect of this quasi-symmetry is not well understood.

[31] The eccentricity variations are less extreme than the inclination variations, but they too are dominated by $\sim$1 Myr variations. In this case the cause is beating between the first and third largest terms, with rates of 5.569 and 4.250 arcsec/year, yielding a beat period of 983 kyr. In this case, the major term is substantially larger than the minor term and the modulation is not as severe as in the inclination history.

[32] Figure 3 illustrates the variations in nodal and apsidal motion over the same 10 million year time span. Here the difference between the relatively regular behavior of the shape of the orbit (e, ϖ) and the quite irregular behavior of orientation of the orbit plane (I, Ω) is clearly evident. The rate of apsidal advance is fairly uniform, the present rate (5.44 arcsec/year) is near to the long term average, and the major variations have a period of roughly 1 Myr. Note that the instantaneous rate of apsidal motion, which includes a famous 0.43 arcsec/year contribution from General Relativity [*Einstein*, 1915; *Roseveare*, 1982; *Nobili and Will*, 1986], also includes short period perturbations which a secular variation model will not capture.

[33] The rate of nodal regression is much more variable. Most of the time it is in the range of -5 to -10 arcsec/yr, with a 230 kyr dominant period of oscillation. However, there are brief intervals during which the node rate changes rapidly. There are even some times when the nodal motion changes direction. These always correspond to episodes when the inclination is small.

5. Linear Spin Model

[34] In this section we develop and apply a simple linearized model of spin pole precession for Mercury. The differential equation which governs the evolution of the spin pole orientation, equation (5), is nonlinear. However, in many cases it has been shown that linear solutions can be obtained which capture many features of the behavior of the system. Such linear models for spin pole evolution have been constructed previously, in the context of studying obliquity variations of the Earth [*Miskovitch*, 1931; *Sharaf and Boudnikova*, 1967; *Vernekar*, 1972; *Berger*, 1976], Mars [*Ward*, 1973, 1992], and Venus [*Ward and de Campli*, 1979; *Yoder and Ward*, 1979; *Yoder*, 1995, 1997].

[35] The first step in that process is to represent the unit vectors $\hat{s}$ and $\hat{n}$, which point along the spin pole and orbit pole, in terms of complex scalars S and N, by projecting
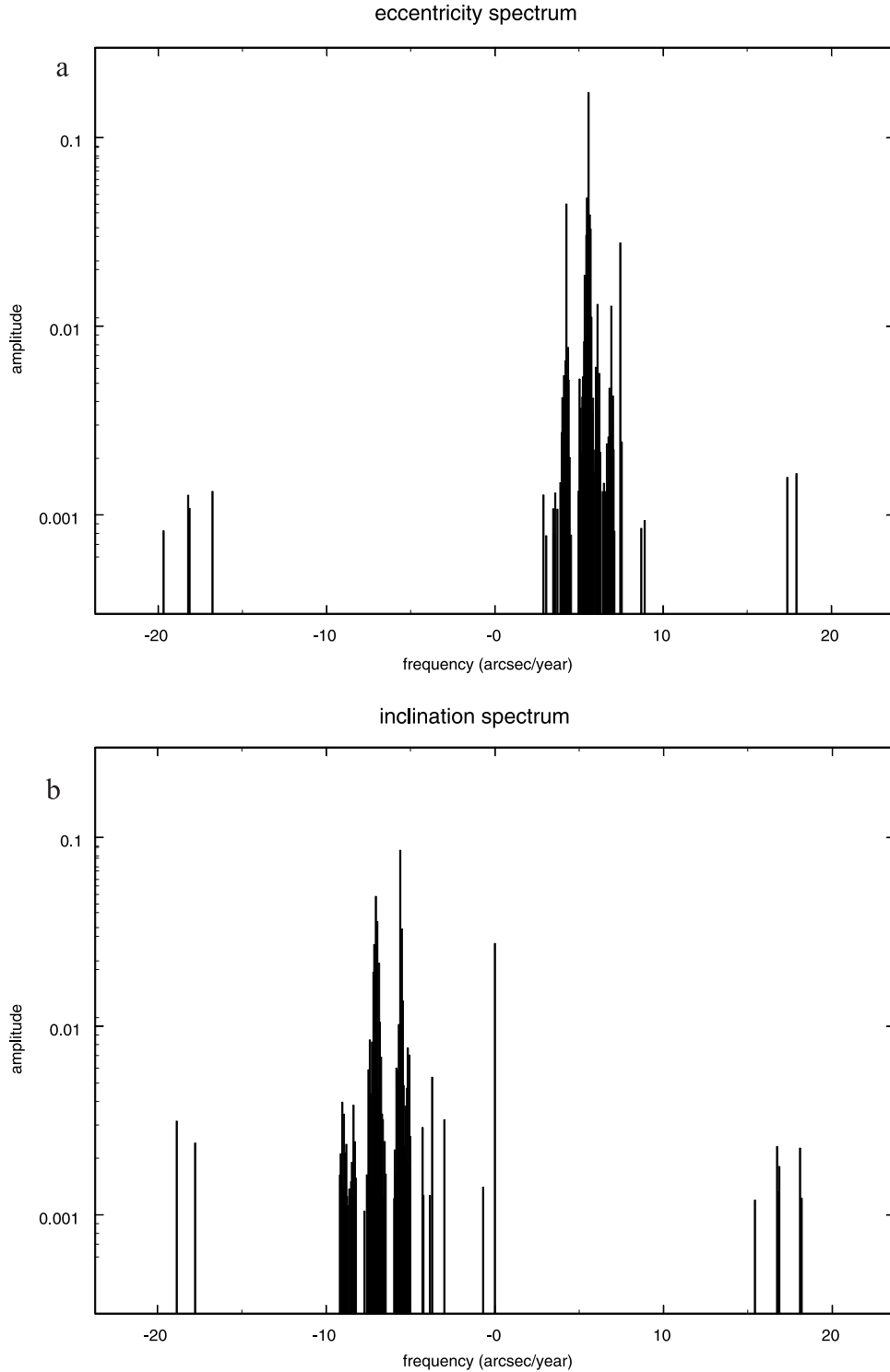
Figure 1. (a) Eccentricity spectrum. The spectrum illustrates amplitudes and rates associated with variations of eccentricity e and longitude of periapse ϖ for the secular variation model of *Laskar* [1988]. (b) Inclination spectrum. The spectrum illustrates amplitudes and rates associated with variations of inclination I and longitude of the node Ω for the secular variation model of *Laskar* [1988].

each of them onto the inertially fixed ecliptic plane of J2000. For example, we represent the spin pole

$$\widehat{n} = \begin{bmatrix} n_1 \\ n_2 \\ n_3 \end{bmatrix} = \begin{bmatrix} \sin I \cos \Omega \\ \sin I \sin \Omega \\ \cos I \end{bmatrix} \qquad (57)$$

by the complex scalar

$$N = n_1 + i\, n_2 = \sin I (\cos \Omega + i \sin \Omega). \qquad (58)$$

In this scheme, and invoking the small angle approximation, we have
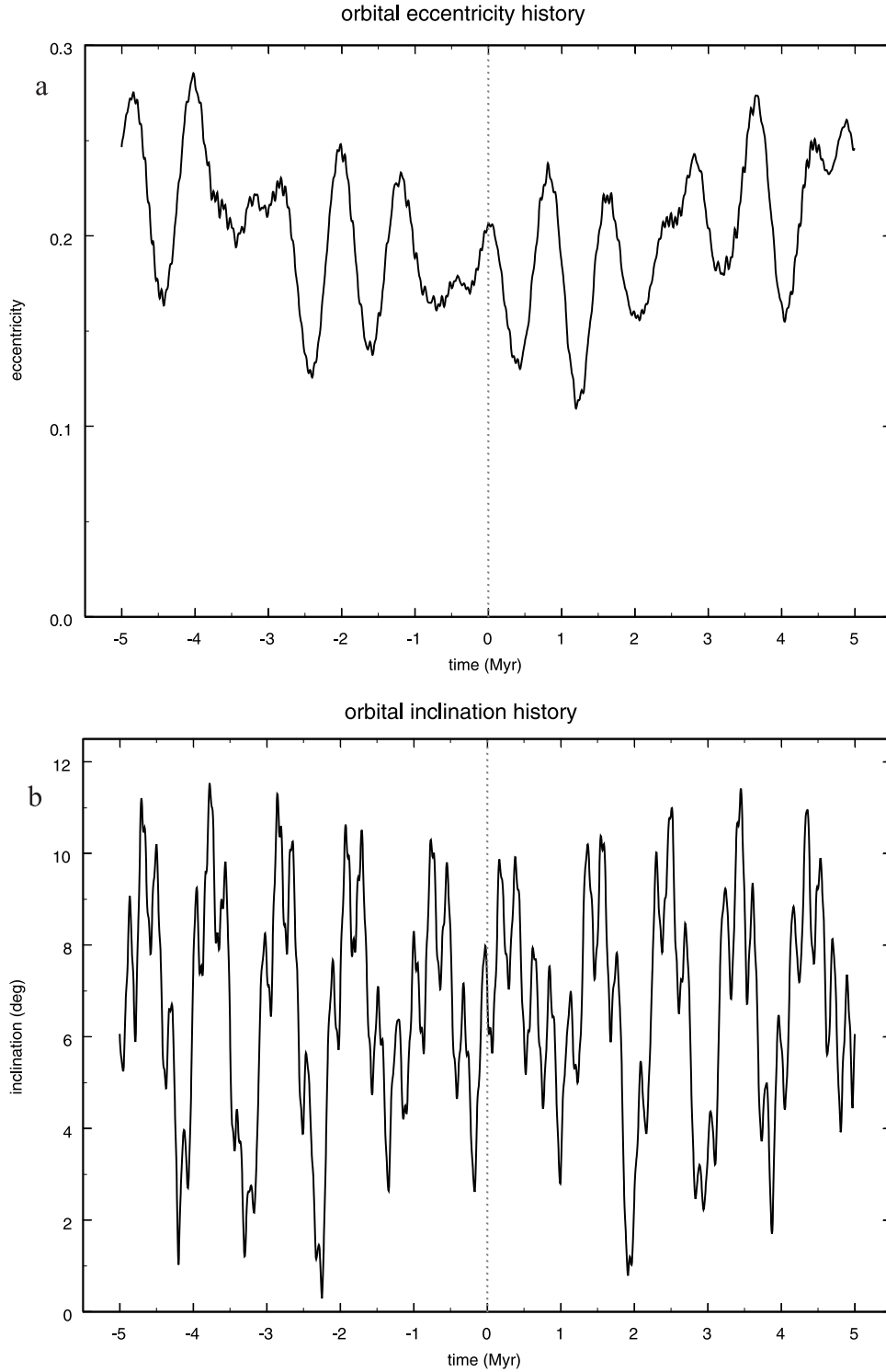
Figure 2. (a) Eccentricity history. Variations in Mercury's orbital eccentricity, from equation (53). (b) Inclination history. Variations in Mercury's orbital inclination, from equation (54). The reference plane is the ecliptic of J2000.

$$\hat{n} \cdot \hat{s} \simeq 1, \tag{59}$$

$$\hat{s} \times \hat{n} \simeq i\,(N - S). \tag{60}$$

The angular separation between the spin pole and orbit pole is the obliquity ε, and their relative azimuth is ψ. Figure 4 illustrates the relative positions of the spin pole and orbit pole, as projected onto the ecliptic plane.
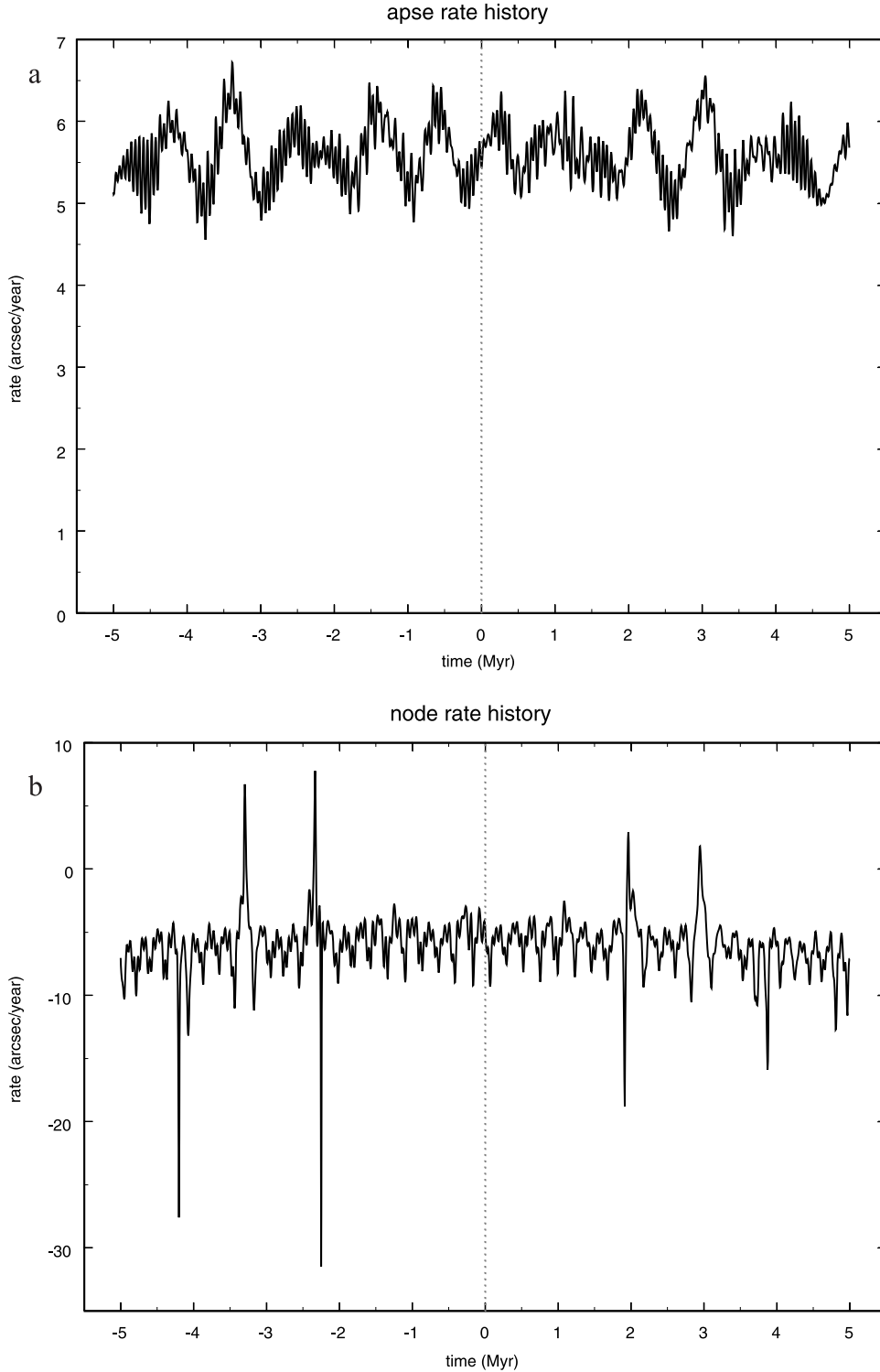
Figure 3. (a) Apse rate history. Variations in the rate of apsidal advance for Mercury's orbit, from equation (55). (b) Node rate history. Variations in the rate of nodal regression for Mercury's orbit, from equation (56).

[36] If we ignore variations in orbital eccentricity, the governing equation for spin pole precession, equation (5), can be written in the simple linear form

$$\frac{dS}{dt} = i\,\alpha\,(N - S). \tag{61}$$

If the orbit pole evolution is represented by the series

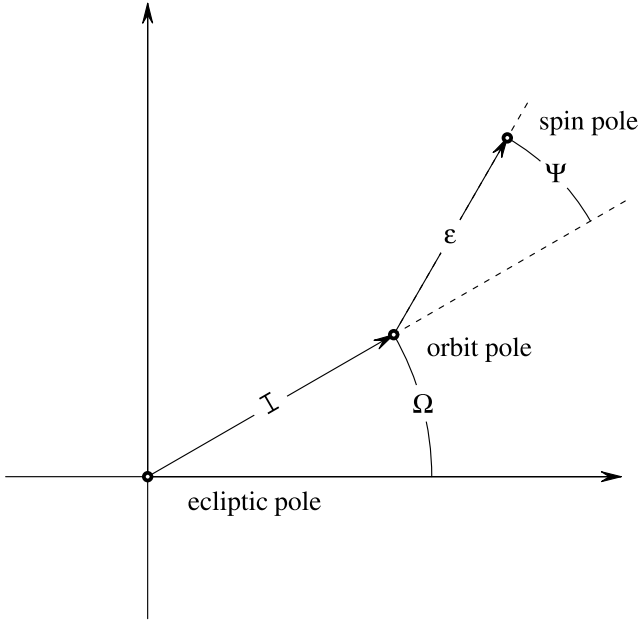$$N[t] = \sum_j F_j\,\exp\big[i\big(f_j t + \phi_j\big)\big], \tag{62}$$

Figure 4. Geometry of spin pole and orbit pole. The unit vectors along the spin pole and orbit pole are both projected onto the fixed ecliptic plane. The orbit pole position is characterized by two angles: inclination I and nodal longitude Ω. The angular displacement between spin and orbit poles is also characterized by two angles: obliquity ε and relative azimuth ψ. The relative size of the obliquity, compared to the inclination, is greatly exaggerated for clarity of presentation.

then the corresponding spin pole evolution can be written simply as

$$S[t] = S_{free} + S_{forced}, \qquad (63)$$

where the free pole motion, which depends only on the initial condition, is

$$S_{free} = S[0] \exp(-i\,\alpha\,t) \qquad (64)$$

and the forced motion is

$$S_{forced} = \sum_j S_j \big(\exp[i f_j t] - \exp[-i\,\alpha\,t] \big) \exp[i\gamma_j], \qquad (65)$$

with amplitudes given by

$$S_j = \left(\frac{\alpha}{\alpha + f_j} \right) F_j. \qquad (66)$$

Each term in the series describing the orbit pole has a corresponding term in the forced spin pole series. The spin rate parameter α is positive, and most of the orbit pole rates f_j are negative. If one of the sums $\alpha + f_j$ is close to zero, then the corresponding amplitude in the spin trajectory will be amplified. However, as we have noted above, the spin pole precession rate parameter α is substantially larger than any of the secular orbital frequencies f_j. As a result, there is no resonant amplification for Mercury. Instead, the spin pole trajectory is essentially a high-pass-filtered version of the orbit pole trajectory.

[37] An apparent difficulty in applying this approach to the spin pole of Mercury is that the initial conditions are not well known. That would be a serious problem for a body like Mars or Earth, where the free obliquity is large. However, tidal dissipation helps in this case, in that the initial conditions are quickly damped out. Dissipation can be easily modeled by making the spin precession parameter complex: $\alpha \rightarrow \alpha + i\beta$.

[38] When included this way, the dissipation completely damps the free term and somewhat modifies the forced terms. Assuming that the damping term is small, the resulting model for damped forced spin evolution takes the form

$$S[t] = \sum_j S_j \big(\exp[i f_j\, t] \big) \exp[i\,\gamma_j]. \qquad (67)$$

The second of the terms in square brackets in the original equation for forced response is removed by dissipation.

[39] The angular separation between spin pole and orbit pole can now be written in a simple form:

$$\Delta S[t] \equiv S[t] - N[t] = \sum_j \Delta S_j\, \exp\big[i\,(f_j\, t + \gamma_j)\big]. \qquad (68)$$

The amplitude of each term is just the difference in amplitudes of the spin and orbit solutions:

$$\Delta S_j = S_j - F_j = \left(\frac{\alpha}{\alpha + f_j} - 1 \right) F_j = \left(\frac{-f_j}{\alpha + f_j} \right) F_j. \qquad (69)$$

[40] This solution can be viewed as an approximate generalization of the Cassini state for the case of nonuniform orbit precession. In the case of uniform orbit precession, the expected end-state for dissipative spin evolution is a special situation in which the obliquity has adjusted to a value at which the system maintains a constant relative geometry. That is, spin pole and orbit pole remain coplanar with the invariable pole as the spin pole precesses about the orbit pole and the orbit pole precesses about the invariable pole [*Colombo*, 1966; *Peale*, 1969; *Ward*, 1975; *Henrard and Murigande*, 1987].

[41] If the orbit pole precession is not steady, no such coplanar configuration is attainable. However, the motions of the orbit and spin poles can achieve a mode-by-mode equivalent of the Cassini state. The solution above is such that each mode of the orbit pole precession, with amplitude F_j, rate f_j, and phase ϕ_j, has a corresponding mode of spin pole precession with rate and phase identical to the orbit mode values, and with an amplitude proportional to the orbit amplitude. The constant of proportionality is just the ratio $\alpha/(\alpha + f_j)$ of the spin precession rate to the relative spin-orbit precession rate.

[42] Figures 5 and 6 provide two different views of the obliquity history of Mercury obtained via this simple linear model and assuming a nominal value of $\alpha = 959$ arcsec/year. Figure 5 shows the motions of the spin pole and orbit pole, both projected onto the ecliptic plane of J2000, for a time span of 3 million years, centered on the present. The coordinate system is inertially fixed, and the horizontal axis in the figure corresponds to the direction
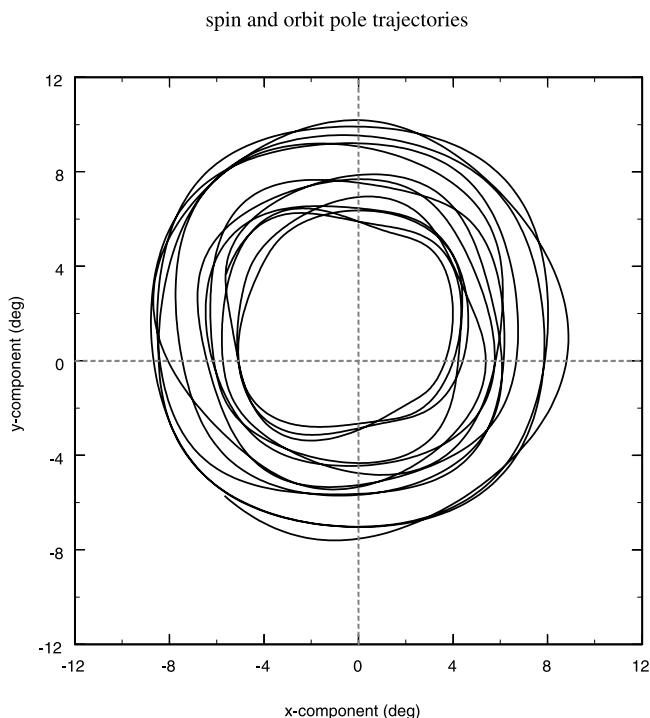
spin and orbit pole trajectories

Figure 5. Trajectories of Mercury spin and orbit poles, projected onto the ecliptic plane of J2000. The coordinate system is as in Figure 4. The maximum separation between the orbit pole and spin pole is less than the line width in this figure. Trajectories span 3 million years, centered on the present.

of the vernal equinox of J2000. At the scale of this figure, the two trajectories are quite indistinguishable. Figure 6 illustrates the obliquity, or angular separation between spin pole and orbit pole, for a time span of 10 million years, also centered on the present. Several features deserve comment. The obliquity history looks very much like a scaled version of the inclination history. The dominant period of obliquity oscillation is the same as for inclination: 895 kyr. In fact, 96% of the variance in the obliquity series is reproduced by a scaled version of the inclination series.

[43] The reason for the nearly linear relationship between inclination and obliquity is that the inclination variations are dominated by the two previously noted spectral lines at rates of −5.604 and −7.053 arcsec/year, and those frequencies are close enough together that the mapping from inclination to obliquity is nearly constant. Despite these similarities, note that the obliquity variations are roughly 200 times smaller than the corresponding inclination variations.

[44] A notable difference in the obliquity series, compared to the inclination series, is the presence of relatively more high-frequency variations in the obliquity. This is readily understood in terms of the high-pass filter discussion above. At longer periods, the spin pole tracks the orbit pole more accurately, and the resulting obliquity variations are attenuated. Higher frequency orbital variations are more clearly expressed in obliquity.

[45] The obliquity trajectories which would be produced via this model using other values of the spin pole precession rate parameter α, are even more nearly just scaled versions of the present obliquity model. If the value of α were changed to 2/3 or 4/3 of the nominal value, which is still
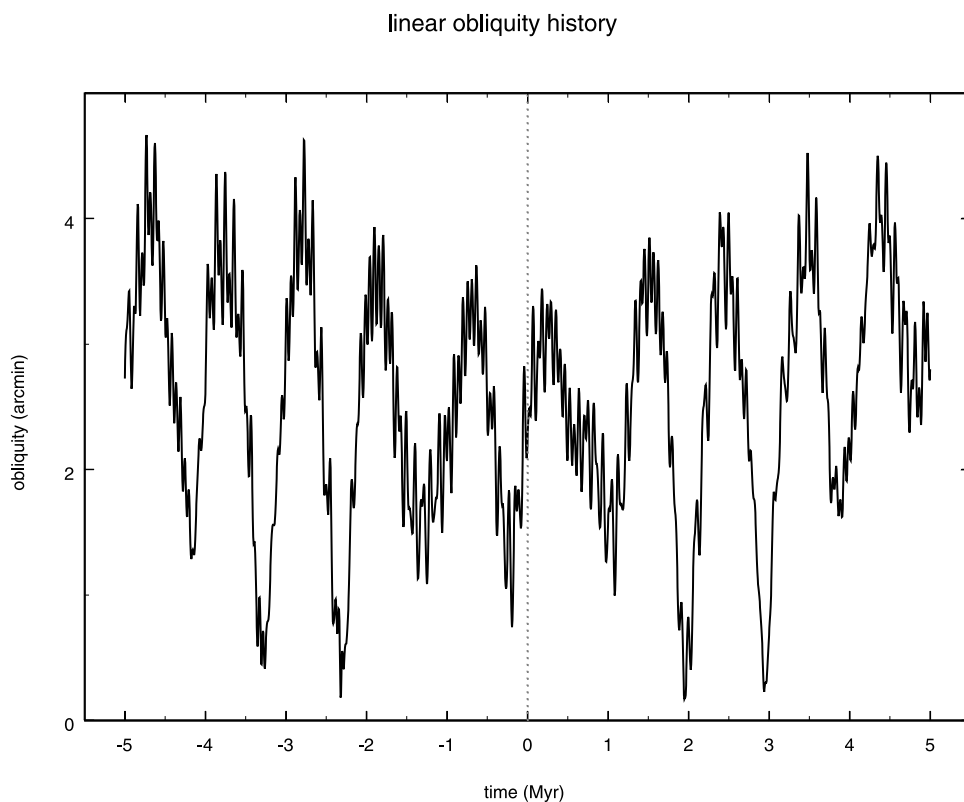
linear obliquity history

Figure 6. Obliquity history. Variations in the obliquity of Mercury, obtained from the linear model of equations (68) and (69), assuming a spin pole precession rate parameter of α = 959 arcsec/year.
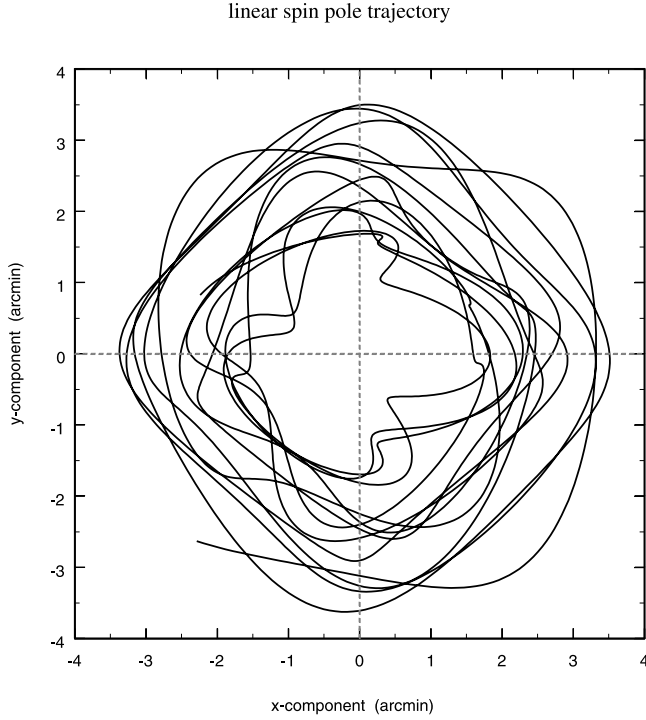
linear spin pole trajectory

Figure 7. Linear model of spin pole and orbit pole relative motion. The unit vector along the spin pole, as reconstructed from the linear model, is projected onto the precessing orbit plane. The quantity plotted is ΔS of equation (70). The time span is 3 million years, centered on the present.

within the current range of uncertainty for that parameter, then the resulting obliquity histories would very nearly approximate 3/2 or 3/4 of the values shown in Figure 4, respectively. Due to the large relative uncertainty in that critical parameter, current reconstructions of the obliquity history for Mercury are quite uncertain. The general shape and spectral character of the obliquity history is rather better known than is the actual value at any particular time.

[46] Figures 7 and 8 provide two additional views of the relative motion of the spin pole and orbit pole. In Figure 7, we show the difference,

$$\Delta S = S - N = \varepsilon \left(\cos(\Omega + \psi) + i \cos(\Omega + \psi) \right), \qquad (70)$$

in positions of the spin pole and orbit pole, as projected onto the ecliptic plane, and as seen in an inertial reference frame. Both the spin pole and the orbit pole are projected onto the plane and then translated so that the orbit pole becomes the new origin. In this view it is clear that the spin pole is precessing around the orbit pole. Note the change in scale between this figure and Figure 5, which uses the same coordinate system. Figure 8 is similar to Figure 7, except that it shows the quantity

$$\delta S = e^{-i\Omega} \Delta S = \varepsilon \left(\cos(\psi) + i \cos(\psi) \right), \qquad (71)$$

which involves a rotation of ΔS through the angle $-\Omega$. If the spin pole and orbit pole remained coplanar with the

fixed ecliptic pole, as would be expected for uniform rates of orbit pole precession, then the spin pole, in this view, would remain on the horizontal axis.

6. Numerical Integration

[47] In this section we examine a numerically integrated solution to the spin precession equation, and compare it with the linearized analysis of the previous section. The linear analysis completely neglects eccentricity variations, and would be expected to perform best when the inclination variations are small. From that perspective, Mercury's obliquity history would appear to be a poor candidate for linearization. However, the spin pole precession rate parameter α is large enough that the spin pole easily tracks motion of the orbit pole, and the obliquity is therefore always quite small. As we will see below, that factor dominates, and makes the linearized model an excellent approximation to the nonlinear behavior of the spin pole trajectory.

[48] In order to evaluate the accuracy of the linearized model for spin pole evolution, we have numerically integrated the full nonlinear equations of motion for the spin pole of Mercury for a time span of 3 million years, centered on the present. The orbital inclination variations in both the linear and nonlinear models come from *Laskar*'s [1988] secular variation model. In the linearized system, we introduced dissipation via an imaginary part to the precession rate parameter α. In the nonlinear equations, we approximate the dissipative effect by writing

$$\frac{d\widehat{s}}{dt} = \left(\alpha_0 + \alpha_2 \, e^2 \right) (\widehat{s} \times \widehat{n}) + \gamma \, (\widehat{n} \cdot \widehat{s}) \, (\widehat{n} - \widehat{s}), \qquad (72)$$
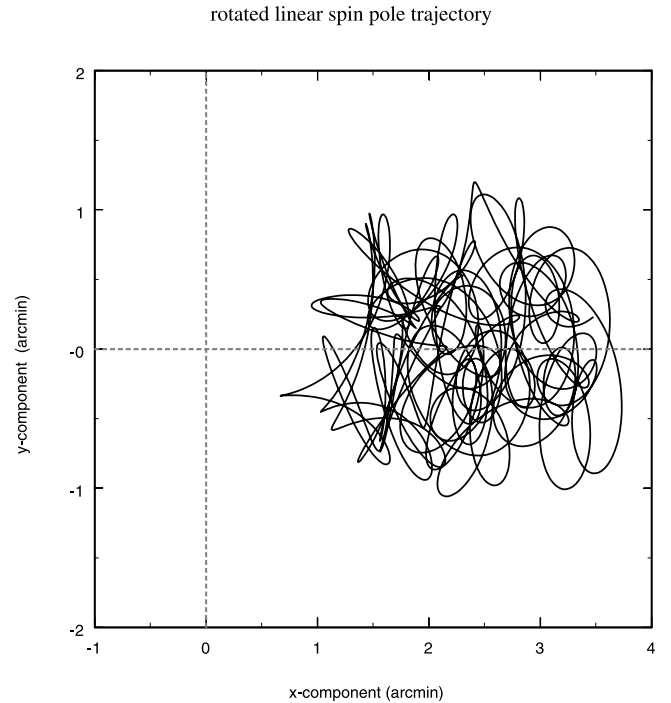
rotated linear spin pole trajectory

Figure 8. Linear model of spin pole and orbit pole relative motion. Similar to Figure 7, except that the quantity plotted is δS of equation (71). The time span is 3 million years, centered on the present.

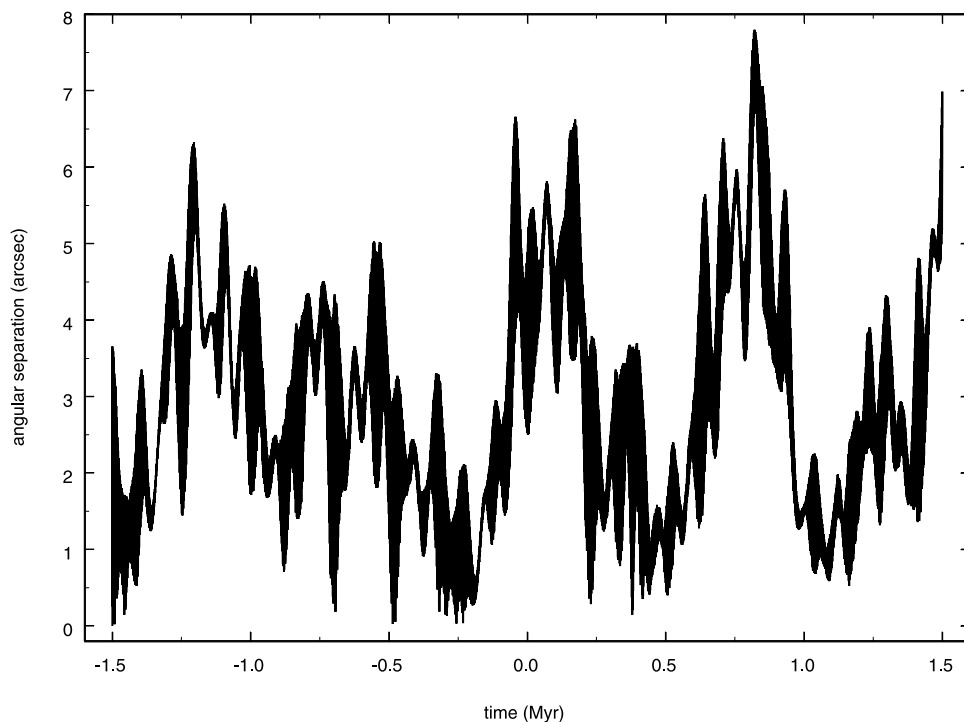distance between linear and nonlinear spin poles

Figure 9. Difference between linear and nonlinear obliquities. Temporal variations in the angular distance between linear and nonlinear spin pole trajectories.

where γ plays a role similar to the imaginary part of α. Numerical values of the damping parameter are difficult to constrain, as they depend on very poorly known material parameters [*deSurgy and Laskar*, 1997; *Touma and Wisdom*, 2001]. We arbitrarily selected a value of

$$\gamma = 10^{-3}\alpha_0, \tag{73}$$

which is almost certainly an overestimate. We integrated this equation, subject to variations in the orbit normal given by (47), (48), (51), and (52), and eccentricity variations given by (45), (46), (49), and (50). For initial conditions, we used the spin pole position estimated from the linearized model at $t = -1.5$ Myr. Plotted at the same scales as Figure 5 or Figure 6, the nonlinear integration would be quite indistinguishable from the linear result. Even at the scale of Figures 7 and 8 the linear and nonlinear trajectories are barely distinguishable. A more discriminating comparison is made in Figure 9, which shows the difference between the linear and nonlinear spin trajectories at 200 year intervals over the complete 3 million year time series. The spin pole is usually within 2–4 arcmin of the orbit pole, and the linear estimate of the spin pole is usually within 2–3 arcsec of the nonlinear estimate.

[49] There is, generally speaking, a very close correspondence between the spin pole trajectory generated via the linear theory and that obtained via numerical integration. The small differences between the trajectories exhibit two different patterns. Over most of the interval examined, the distance between the two spin poles varies with dominant periods of roughly 10^5 and 10^6 years, which are the

principal periods on which the obliquity itself varies. Part of that variation is simply due to the fact that the linear model neglects orbital eccentricity. As the eccentricity changes, so too does the effective spin pole precession rate. Thus the optimum angular separation between spin pole and orbit pole, at which they can remain coplanar with the invariable pole, will slowly vary.

[50] This behavior clearly illustrates an important difference between purely inertial systems and those with damping. It has been argued [*Laskar and Robutel*, 1993; *Touma and Wisdom*, 1993] that several of the planets exhibit chaotic obliquity variations. A distinguishing feature of chaotic motion is that nearby trajectories exhibit exponential divergence. For Mercury, in the presence of substantial tidal dissipation, the opposite is true. Though our simulation had short episodes during which the nonlinear trajectory diverged slightly from the linear trajectory, it was subsequently attracted back to the linear trajectory. This behavior is quite characteristic of nonlinear dynamical systems with dissipation [*Gray et al.*, 1998; *Chacon*, 1999].

[51] In the case of uniform orbital precession, it has been shown [*Colombo*, 1966; *Peale*, 1969; *Ward*, 1975; *Henrard and Murigande*, 1987] that there are either 2 or 4 stable equilibrium configurations, in which the spin pole and orbit pole maintain fixed relative positions. The number of equilibria (either 2 or 4), and which of them a system is attracted to, depend on system parameters and initial conditions. In the case of nonuniform orbit precession, no such global solution has been demonstrated. However, the damped linear analysis presented above yields a solution

which is apparently stable and is, at least locally, an attractor.

[52] In his analysis of the obliquity of Mercury, *Peale* [1974] mainly considered the case in which the orbital eccentricity is fixed and the orbit plane is precessing at a uniform rate. However, on the basis of an earlier analysis by *Goldreich and Toomre* [1969], Peale argued that the temporal variations in eccentricity or precession rate would only induce small departures of the spin pole from the Cassini state, as long as those variations were slow, compared to the spin pole precession rate. The argument is essentially that the solid angle swept out by the instantaneous spin pole, as it precesses about the Cassini state, will be an adiabatic invariant. Peale estimated that variations in orbital eccentricity and inclination, associated with the single spectral line near 10^5 year period, would drive departures of the spin pole from the Cassini state of about 5 arcsec. Our simulations are consistent with this rough estimate. Though we find larger variations, they include contributions from several different forcing periods, and are dominated by the inclination variations at 10^6 year period.

7. Summary and Discussion

[53] We have developed and applied a simple model of the secular variations in obliquity for Mercury. The linear model performs very well, when compared with a nonlinear numerical integration of the equations of motion. The primary limitation on reconstructing obliquity variations over time scales of order 10 million years is the large uncertainty in the gravitational oblateness of the planet. That limitation will likely be removed when spacecraft are placed into orbit about Mercury, in the near future. On still longer time scales, uncertainties in the orbital motion become a limiting error source.

[54] Our analysis suggests that tidal dissipation has likely driven Mercury into a dynamical state which shares some features with the Cassini state that the Moon occupies, but also differs from it in other regards. Whereas the lunar orbit pole and spin pole remain very nearly coplanar with the pole of the ecliptic, as the spin pole and orbit pole both precess, the nonuniform orbital precession rate of Mercury precludes a coplanar configuration for its spin pole, orbit pole, and solar system invariable pole. However, when the spin pole and orbit pole trajectories are analyzed in terms of the secular normal modes of oscillation of the solar system, it is seen that the coplanar configuration holds on a mode-by-mode basis. This represents an important generalization of the concept of Cassini states to situations with nonuniform orbital precession.

[55] The primary pattern of obliquity variations for Mercury is less sensitively dependent on the gravitational oblateness than is the case for Mars, for example, since Mercury's spin pole precession rate is much faster than any of the secular orbital variations. The present obliquity is expected to be near to 1.8 minutes of arc. The primary temporal variations have periods of ~100 kyr and ~1 Myr. Ironically, some of the measurement objectives of the MESSENGER and BepiColombo missions will be considerably easier than if they had been launched 180,000 years ago, when the obliquity was at a local minimum value. On the other hand, waiting another 70,000 years, until a local maximum in obliquity occurs, would make the measurements still easier.

References

Anderson, J. D., G. Colombo, P. B. Espositio, E. L. Lau, and G. B. Trager (1987), The mass, gravity field and ephemeris of Mercury, *Icarus*, *71*, 337–349.

Anderson, J. D., R. F. Jurgens, E. L. Lau, and M. A. Slade (1996), Shape and orientation of Mercury from radar ranging data, *Icarus*, *124*, 690–697.

Anselmi, A., and G. E. N. Scoon (2001), BepiColombo, ESA's Mercury Cornerstone mission, *Planet. Space Sci.*, *49*, 1409–1420.

Balogh, A., and G. Giampieri (2002), Mercury: The planet and its orbit, *Rep. Prog. Phys.*, *65*, 529–560.

Berger, A. L. (1976), Obliquity and precession for the last 5 million years, *Astron. Astrophys.*, *51*, 127–135.

Bills, B. G. (1990), The rigid body obliquity history of Mars, *J. Geophys. Res.*, *95*, 14,137–14,153.

Brouwer, D., and A. J. J. van Woerkom (1950), The secular variations of the orbital elements of the principal planets, *Astron. Pap. Am. Ephem.*, *13*, 81–107.

Carpentier, G., and F. Roosbeek (2003), Analytic development of rigid Mercury nutation series, *Celest. Mech. Dynam. Astron.*, *86*, 223–236.

Cassini, G. D. (1693), Traité de l'origine et du Progrés de l'Astronomie, R. Acad. of Sci., Paris.

Cayley, A. (1861), Tables of the developments of functions in the theory of elliptic motion, *Mem. R. Astron. Soc.*, *29*, 191–306.

Chacon, R. (1999), General results on chaos suppression for biharmonically driven dissipative systems, *Phys. Lett. A*, *257*, 293–300.

Chirikov, B. V. (1979), A universal instability of many dimensional oscillator systems, *Phys. Rep.*, *52*, 263–379.

Colombo, G. (1966), Cassini's second and third laws, *Astron. J.*, *71*, 891–896.

Colombo, G., and I. I. Shapiro (1966), The rotation of the planet Mercury, *Astrophys. J.*, *145*, 296–307.

Counselman, C. C. (1969), Spin-orbit resonance of Mercury, Ph.D. thesis, Mass. Inst. of Technol., Cambridge.

Deprit, A., and E. Deprit (1990), Processing Poisson series in parallel, *J. Symb. Comput.*, *10*, 179–201.

deSurgy, O. N., and J. Laskar (1997), On the long term evolution of the spin of the earth, *Astron. Astrophys.*, *318*, 975–989.

Einstein, A. (1915), Erklärung der Perihelbewegung des Merkur aus der allgemeinen Relativitätstheorie, *Preuss. Akad. Wiss. Berlin*, *47*, 831–839.

Folkner, W. M., C. F. Yoder, D. N. Yuan, E. M. Standish, and R. A. Preston (1997), Interior structure and seasonal mass redistribution of Mars from radio tracking of Mars Pathfinder, *Science*, *278*, 1749–1752.

Goldreich, P., and S. J. Peale (1966), Spin-orbit coupling in the solar system, *Astron. J.*, *71*, 425–438.

Goldreich, P., and S. J. Peale (1968), Dynamics of planetary rotations, *Annu. Rev. Astron. Astrophys.*, *6*, 287–320.

Goldreich, P., and A. Toomre (1969), Some remarks on polar wandering, *J. Geophys. Res.*, *74*, 2555–2567.

Gray, G. L., A. P. Mazzoleni, and D. R. Campbell (1998), Analytical criterion for chaotic dynamics in flexible satellites with nonlinear controller damping, *J. Guidance Control Dyn.*, *21*, 558–565.

Harder, H., and G. Schubert (2001), Sulfur in Mercury's core?, *Icarus*, *151*, 118–122.

Harmon, J. K., P. J. Perillat, and M. A. Slade (2001), High-resolution radar imaging of Mercury's north pole, *Icarus*, *149*, 1–15.

Henrard, J. (1989), A survey of Poisson series processors, *Celest. Mech.*, *45*, 245–253.

Henrard, J., and C. Murigande (1987), Colombo's top, *Celest. Mech*, *40*, 345–366.

Holin, I. V. (2002), Radar speckle displacement interferometry for precision measurement of obliquity and physical librations of Mercury, *Sol. Syst. Res.*, *36*, 206–213.

Hughes, S. (1981), The computation of tables of Hansen coefficients, *Celest. Mech.*, *25*, 101–107.

Ito, T., and K. Tanikawa (2002), Long-term integrations and stability of planetary orbits in our solar system, *Mon. Not. R. Astron. Soc.*, *336*, 483–500.

Kinoshita, H. (1977), Theory of rotation of the rigid Earth, *Celest. Mech.*, *15*, 277–326.

Klaasen, K. P. (1976), Mercury's rotation axis and period, *Icarus*, *28*, 469–478.

Laskar, J. (1988), Secular evolution of the solar system over 10 million years, *Astron. Astrophys.*, *198*, 341–362.

Laskar, J. (1990), The chaotic motion of the solar system: A numerical estimate of the size of the chaotic zones, *Icarus*, *88*, 266–291.

Laskar, J. (1994), Large-scale chaos in the solar system, *Astron. Astrophys.*, *287*, L9–L12.

Laskar, J., and P. Robutel (1993), The chaotic obliquity of the planets, *Nature*, *361*, 608–612.

Lecar, M., F. A. Franklin, M. J. Holman, and N. W. Murray (2001), Chaos in the solar system, *Annu. Rev. Astron. Astrophys.*, *39*, 581–631.

Lissauer, J. J. (1999), Chaotic motion in the solar system, *Rev. Mod. Phys.*, *71*, 835–845.

McCarthy, D. D., and B. J. Luzum (2003), An abridged model of the precession-nutation of the celestial pole, *Celest. Mech. Dyn. Astron.*, *85*, 37–49.

Milani, A., A. Rossi, D. Vokrouhlicky, D. Villani, and C. Bonanno (2001), Gravity field and rotation state of Mercury from the BepiColombo Radio Science Experiments, *Planet. Space Sci.*, *49*, 1579–1596.

Miskovitch, V. V. (1931), Variations seculaires de elements astronomiques de l'orbite terrestre, *Glas. Spr. Kal'yevske Acad.*, 143.

Morbidelli, A. (2002), Modern integrations of solar system dynamics, *Annu. Rev. Earth Planet. Sci.*, *30*, 89–112.

Murray, C. D., and S. F. Dermott (1999), *Solar System Dynamics*, 592 pp., Cambridge Univ. Press., New York.

Navarro, J. F., and J. M. Ferrándiz (2002), A new symbolic processor for the Earth rotation theory, *Celest. Mech. Dyn. Astron.*, *82*, 243–263.

Nobili, A. M., and C. M. Will (1986), The real value of Mercury's perihelion advance, *Nature*, *320*, 39–41.

Peale, S. J. (1969), Generalized Cassini's laws, *Astron. J.*, *74*, 483–489.

Peale, S. J. (1974), Possible histories of the obliquity of Mercury, *Astron. J.*, *79*, 722–744.

Peale, S. J. (1976), Inferences from dynamical history of Mercury's rotation, *Icarus*, *28*, 459–467.

Peale, S. J., and A. P. Boss (1977a), A spin-orbit constraint on the viscosity of a Mercurian liquid core, *J. Geophys. Res.*, *82*, 743–749.

Peale, S. J., and A. P. Boss (1977b), Mercury's core-effect of obliquity on spin-orbit constraints, *J. Geophys. Res.*, *82*, 3423–3429.

Peale, S. J., R. J. Phillips, S. C. Solomon, D. E. Smith, and M. T. Zuber (2002), A procedure for detemining the nature of Mercury's core, *Meteorit. Planet. Sci.*, *37*, 1269–1283.

Pettengill, G., and R. B. Dyce (1965), A radar determination of rotation of planet Mercury, *Nature*, *206*, 1240–1242.

Rambaux, N., and E. Bois (2004), Theory of the Mercury's spin-orbit motion and analysis of its main librations, *Astron. Astrophys.*, *413*, 381–393.

Roseveare, N. T. (1982), *Mercury's Perihelion From Le Verrier to Einstein*, 208 pp., Oxford Univ. Press, New York.

San Juan, F., and A. Abad (2001), Algebraic and symbolic manipulation of Poisson series, *J. Symb. Comput.*, *32*, 565–572.

Schubert, G., M. N. Ross, D. J. Stevenson, and T. Spohn (1988), Mercury's thermal history and generation of its magnetic field, in *Mercury*, edited by F. Vilas, C. R. Chapman, and M. S. Mathews, pp. 429–460, Univ. of Ariz. Press, Tucson.

Sharaf, S. G., and N. A. Boudnikova (1967), Secular variations of elements of the Earth's orbit which influence climates of the geological past, *Bull. Inst. Theor. Astron.*, *11*, 231–261.

Solomon, S. C., et al. (2001), The MESSENGER mission to Mercury: Scientific objectives and implementation, *Planet. Space Sci.*, *49*, 1445–1465.

Spohn, T., F. Sohl, K. Wieczerkowski, and V. K. Conzelmann (2001), The interior structure of Mercury: What we know, what we expect from BepiColombo, *Planet. Space Sci.*, *49*, 1561–1570.

Standish, E. M., X. X. Newhall, J. G. Williams, and D. K. Yeomans (1992), Orbital ephemerides of the Sun, Moon, and planets, in *Explanatory Supplement to the Astronomical Almanac*, edited by P. K. Seidelmann, pp. 279–382, Univ. Sci., Mill Valley, Calif.

Sussman, G. J., and J. Wisdom (1992), Chaotic evolution of the solar system, *Science*, *257*, 56–62.

Touma, J., and J. Wisdom (1993), The chaotic obliquity of Mars, *Science*, *259*, 1294–1296.

Touma, J., and J. Wisdom (2001), Nonlinear core-mantle coupling, *Astron. J.*, *122*, 1030–1050.

Vakhidov, A. A. (2001), Some recurrence relations between Hansen coefficients, *Celest. Mech. Dyn. Astron.*, *81*, 177–190.

Vernekar, A. D. (1972), Long period global variations of incoming solar radiation, *Meteorol. Monogr.*, *12*, 1–22.

Ward, W. R. (1973), Large scale variations in the obliquity of Mars, *Science*, *181*, 260–262.

Ward, W. R. (1975), Tidal friction and generalized Cassini's laws in the solar system, *Astron. J.*, *80*, 64–70.

Ward, W. R. (1992), Long-term orbital and spin dynamics of Mars, in *Mars*, edited by H. H. Kieffer et al., pp. 298–320, Univ. of Ariz. Press, Tucson.

Ward, W. R., and W. M. deCampli (1979), Comments on the Venus rotation pole, *Astrophys. J. Lett.*, *230*, L117–L121.

Ward, W. R., and D. J. Rudy (1991), Resonant obliquity of Mars, *Icarus*, *94*, 160–164.

Williams, J. G. (1994), Contributions to the Earth's obliquity rate, precession and nutation, *Astron. J.*, *108*, 711–724.

Winter, O. C., and C. D. Murray (1997a), Resonance and chaos. 1. First-order interior resonances, *Astron. Astrophys.*, *319*, 290–304.

Winter, O. C., and C. D. Murray (1997b), Resonance and chaos. 2. Exterior resonances and asymmetric libration, *Astron. Astrophys.*, *328*, 399–408.

Wisdom, J. (1980), The resonance overlap criterion and the onset of stochastic behavior in the restricted 3-body problem, *Astron. J.*, *85*, 1122–1133.

Wisdom, J. (1987), Chaotic dynamics in the solar system, *Icarus*, *72*, 241–275.

Yoder, C. F. (1995), Venus' free obliquity, *Icarus*, *117*, 250–286.

Yoder, C. F. (1997), Venusian spin dynamics, in *Venus II: Geology, Geophysics, Atmosphere, and Solar Wind Environment*, edited by S. W. Bougher, D. M. Hunten, and R. J. Phillips, pp. 1087–1124, Univ. of Ariz. Press, Tucson.

Yoder, C. F., and W. R. Ward (1979), Does Venus wobble?, *Astrophys. J.*, *233*, L33–L37.

Yoder, C. F., A. S. Konopliv, D. N. Yuan, E. M. Standish, and W. M. Folkner (2003), Fluid core size of Mars from detection of the solar tide, *Science*, *300*, 299–303.

———————————

B. G. Bills and R. L. Comstock, Scripps Institution of Oceanography, La Jolla, CA 92093-0225, USA. (bbills@ucsd.edu)